Structural analysis of the inactive state of the *Escherichia coli* DNA polymerase clamp-loader complex

Steven L. Kazmirski*†‡, Marjetka Podobnik*‡§, Tanya F. Weitze*†, Mike O'Donnell¶, and John Kuriyan*†‖

*Department of Molecular and Cell Biology and Department of Chemistry, Howard Hughes Medical Institute, University of California, Berkeley, CA 94720; †Physical Biosciences Division, Lawrence Berkeley National Laboratory, Berkeley, CA 94720; and ¶Howard Hughes Medical Institute, The Rockefeller University, New York, NY 10021

Contributed by John Kuriyan, October 22, 2004

Clamp-loader complexes are heteropentameric AAA+ ATPases that load sliding clamps onto DNA. The structure of the nucleotide-free *Escherichia coli* clamp loader had been determined previously and led to the proposal that the clamp-loader cycles between an inactive state, in which the ATPase domains form a closed ring, and an active state that opens up to form a "C" shape. The crystal structure was interpreted as being closer to the active state than the inactive state. The crystal structure of a nucleotide-bound eukaryotic clamp loader [replication factor C (RFC)] revealed a different and more tightly packed spiral organization of the ATPase domains, raising questions about the significance of the conformation seen earlier for the bacterial clamp loader. We describe crystal structures of the *E. coli* clamp-loader complex bound to the ATP analog ATPγS (at a resolution of 3.5 Å) and ADP (at a resolution of 4.1 Å). These structures are similar to that of the nucleotide-free clamp-loader complex. Only two of the three functional ATP-binding sites are occupied by ATPγS or ADP in these structures, and the bound nucleotides make no interfacial contacts in the complex. These results, along with data from isothermal titration calorimetry, molecular dynamics simulations, and comparison with the RFC structure, suggest that the more open form of the *E. coli* clamp loader described earlier and in the present work corresponds to a stable inactive state of the clamp loader in which the ATPase domains are prevented from engaging the clamp in the highly cooperative manner seen in the fully ATP-loaded RFC-clamp structure.

AAA+ ATPase | clamp loader | DNA polymerase III | DNA replication | replication factor C

Chromosomal replicases in all of the branches of life achieve high processivity by tethering their catalytic subunits to sliding DNA clamps (1–3). The closed circular sliding clamps are loaded onto DNA by ATP-dependent clamp-loader complexes (4), which are conserved heteropentameric ATPase assemblies. Most sliding clamps are stable closed rings in solution, although recent studies suggest that the clamp in T4 bacteriophage may be open in solution and that the role of the clamp loader might be to stabilize the open form and guide it to DNA (5). The subunits of the clamp-loader complexes consist of three conserved domains, with the first two being closely related to the nucleotide-binding domains of AAA+ ATPases (6–10). The AAA+ domains of the clamp loader are suspended loosely from a circular helical collar that is formed by the third (C-terminal) domains.

ATP binding to the clamp loader triggers a conformational change that allows the complex to bind to and open the clamp and load it onto DNA (11, 12). In an intriguing control mechanism, the interaction with DNA stimulates the otherwise suppressed ATPase activity of the clamp loader, leading to ATP hydrolysis (11, 13) and separation of the clamp-loader complex from the DNA-loaded clamp. How ATP binding is coupled to loading of the clamp on DNA is poorly understood, and elucidating the molecular steps of this process is of interest not only because of its central role in replication but also because of the widespread use of AAA+ ATPases in biology (8).

The crystal structure of the *Escherichia coli* clamp-loader complex (γ complex) has been determined in the absence of nucleotides (6). Three of the five subunits of this clamp loader are functional ATPases (γ_B, γ_C, and γ_D, where B–D refer to the position of the subunit in the assembly; Fig. 1). The two other subunits of the clamp loader (δ_A and δ'_E) do not bind nucleotides. The δ_A-subunit can bind to and open the clamp on its own, and the crystal structure of an isolated *E. coli* δ-subunit bound to an open form of the β clamp has been determined (14). If we model the interaction between the intact clamp loader and the β clamp by docking the N-terminal domain of the δ_A-subunit onto the β clamp based on the crystal structure of the δ:β complex (14), major overlaps between the clamp-loader subunits C–E and the β clamp are observed (6). Although the N terminus of the δ_A-subunit is quite exposed in this clamp-loader structure, the inability to dock the β clamp without collision is consistent with the inactive nature of the nucleotide-free clamp loader that was crystallized. Nevertheless, the highly asymmetric and splayed-out arrangement of the AAA+ domains and the flexible linkage of the AAA+ modules to the main body of the clamp loader led to the suggestion that crystal-packing forces might have distorted the structure and that the inactive form might have the critical δ_A-subunit more completely sequestered within a closed and more symmetrical conformation of the clamp-loader complex (Fig. 1*B*) (6).

The crystal structure of the nucleotide-free clamp loader has two of the ATP-binding sites wide open and one sealed shut by the close juxtaposition of the adjacent two subunits. Inspired by the circular rings formed by most AAA+ ATPases (9, 10), we had speculated that in the absence of nucleotide the clamp-loader complex might snap into a hypothetical "closed" conformation in which each of the nucleotide-binding sites is sealed and the AAA+ domains of δ_A and δ'_E are bound to each other. We reasoned that the binding energy of ATP might be used to pry apart the δ_A- and δ'_E-subunits, allowing δ_A to interact with and open the β clamp (6). This model emphasized the cyclical release and sequestration of the δ_A-subunit, because biochemical data demonstrate that although the isolated δ-subunit binds to the β clamp, the interaction of the assembled clamp-loader complex with the clamp is ATP-dependent (12, 15). Recently, fluorescence resonance energy transfer experiments revealed little change in the distance between the N-terminal domains of δ_A and δ'_E after nucleotide or β-clamp binding (16). These results

---

Freely available online through the PNAS open access option.

Abbreviations: RFC, replication factor C; ITC, isothermal titration calorimetry; MD, molecular dynamics.

Data deposition: The atomic coordinates and structure factors have been deposited in the Protein Data Bank, www.pdb.org (PDB ID codes 1XXH and 1XXI).

‡S.L.K. and M.P. contributed equally to this work.

§Present address: National Institute of Chemistry, Laboratory for Biosynthesis and Biotransformation, P.O. Box 660, Hajdrihova 19, 1001 Ljubljana, Slovenia.

‖To whom correspondence should be addressed. E-mail: kuriyan@berkeley.edu.

www.pnas.org/cgi/doi/10.1073/pnas.0407904101

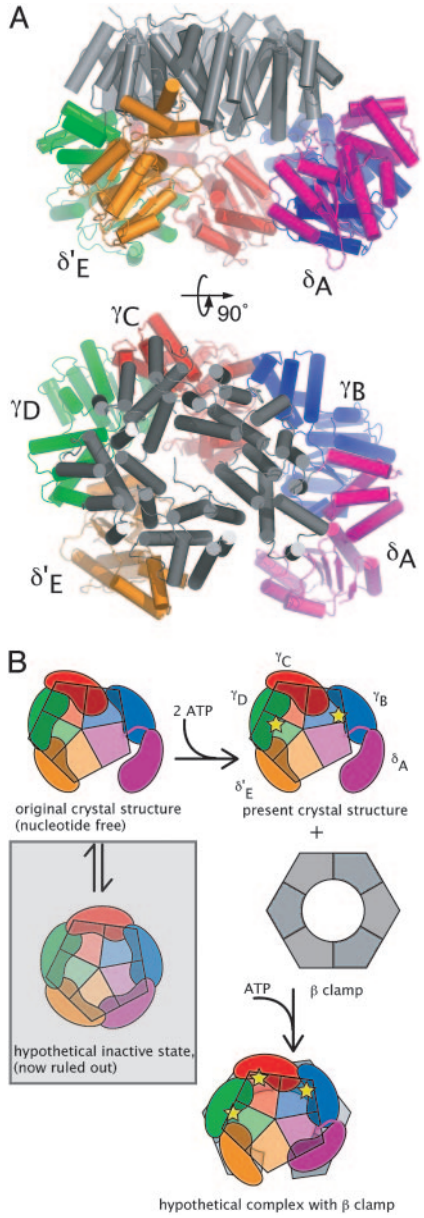

Fig. 1. Structure of the clamp-loader complex. (*A*) Two views of the structure of the ATPγS complex. The A subunit is δ, which is primarily responsible for opening the β clamp. The ATP-binding subunits, γ, are labeled B–D. The E subunit is δ′. (*B*) Schematic diagram showing a suggested mechanism for β clamp binding by the clamp-loader complex. Illustrations of protein structures were generated by using PYMOL (43).

suggest that the shift from a closed form to a more open conformation is unlikely to be a major component of the activation process.

The structure of the eukaryotic clamp-loader complex, replication factor C (RFC), has been determined in complex with ATPγS and the sliding-clamp, proliferating cell nuclear antigen (17). Unexpectedly, the ATP-bound form of the clamp loader is seen to adopt a spiral structure, with its A, B, and C subunits making contact with proliferating cell nuclear antigen. Despite the quite distinct conformation of the RFC complex, there is not a large difference in the distance between the A and E subunits between the nucleotide-free *E. coli* clamp loader and the RFC complex, suggesting again that the transition from an inactive form of the clamp loader may be quite different from that envisaged earlier.

The conformation of the RFC complex suggests a model for how primed DNA is recognized by the clamp–clamp-loader complex (17). In this model, the ATPase domains of the clamp loader wrap around duplex DNA, and the gap created by the "missing" sixth subunit (present in most AAA^+ ATPases but missing in clamp loaders) allows the single-stranded template DNA to exit the inner chamber of the clamp loader. A recent electron microscopy study of an archaeal clamp-loader, clamp–DNA complex suggests that the DNA exits through the opening in the center of the helical collar (18). We recently carried out an analysis of DNA binding by the *E. coli* clamp loader in which we mutated residues that are predicted by the RFC model to interact with DNA (E. Goedken and J.K., unpublished data), and our results suggest that general features of ATP binding and DNA recognition are likely to be conserved between the *E. coli* and eukaryotic clamp loaders. Therefore, it is likely that the *E. coli* clamp loader adopts a spiral conformation when fully loaded with ATP and bound to the clamp and DNA, which raises the question as to the significance of the original structure of the nucleotide-free conformation of the *E. coli* clamp loader.

We have determined the structure of the *E. coli* clamp-loader complex in the presence of the poorly hydrolyzable ATP analog ATPγS at a resolution of 3.5 Å and in the presence of ADP at a 4.1-Å resolution. Despite the low resolution of the crystallographic analyses, these structures show that the overall conformation of these nucleotide-bound forms of the clamp loader is essentially the same as that described earlier in the absence of nucleotides. Only two of the three ATP-binding sites are occupied in these structures, at binding sites that are completely accessible, with no interfacial interactions that could distinguish between ATP or ADP. Isothermal titration calorimetry (ITC) analyses of ATP binding are consistent with the crystal structure and suggest that, in the absence of the β clamp, only two molecules of ATP may be bound to the clamp loader. Molecular dynamics (MD) simulations show that the conformation of the clamp loader seen in the original crystal structure and in the new crystal forms is stable in the absence of nucleotides, suggesting that the original structure may not be significantly distorted by crystal-packing forces. We interpret these results to mean that the highly asymmetric and splayed-open structure of the clamp loader, seen earlier and recapitulated here, represents a stable inactive state of the clamp loader. Transition to the active form most likely requires the remodeling of the base of the clamp loader so that its shape is complementary to that of the clamp.

Materials and Methods

Structure Determination. The *E. coli* clamp-loader complex was prepared as described (15) by using a truncated form of the γ-subunit (residues 1–373). Preparation of δ- and δ′-subunits containing selenomethionine followed similar procedures, with the following exceptions. *E. coli* B834 (DE3) (Novagen) cells were grown in M9 minimal medium, which contained 50 mg/liter of all of the amino acids except methionine. A selenomethionine (Calbiochem) stock solution of 10 mg/ml in water was added to the medium to a concentration of 50 mg/liter. Selenomethionine (five residues in δ and six residues in δ′) was incorporated to ≈100%, as confirmed by mass spectrometry.

The purified clamp-loader complex was concentrated to 10 mg/ml in 20 mM Tris·HCl, pH 7.5/2 mM DTT by ultrafiltration (Millipore). $MgCl_2$, ATPγS, and ADP stock solutions in 50 mM Tris·HCl (pH 7.5) were added to the sample for final concentrations of 16 and 4 mM, respectively, and allowed to incubate on ice for 1 h. The final protein concentration was ≈80 mg/ml. Crystals of the clamp-loader complex with ATPγS were first obtained in 20% polyethylene glycol 3350 and 200 mM Na_2HPO_4 at 20°C. These crystals were then crushed and used as seeds to grow crystals from 8% polyethylene glycol 3350/100 mM Na_2HPO_4/150 mM Hepes, pH 7.95/10% of the detergent Anapoe X-405 (Hampton Research,

Table 1. Crystallographic data statistics

	ATPγS crystals			
	λ1	λ2	λ3	ADP crystals
X-ray wavelength, Å	0.9641	0.9797	0.9795	1.0000
Resolution, Å	100–3.45	100–3.8	100–3.9	100–4.1
No. of reflections	368,979	332,036	215,479	329,382
No. of unique reflections	73,704	51,623	50,659	45,400
R_{sym}	0.100 (0.504)	0.138 (0.583)	0.123 (0.522)	0.096 (0.475)
Completeness, %	97.8 (86.6)	91.2 (61.7)	94.8 (59.2)	94.0 (83.5)
I/σ	15.1 (2.1)	12.2 (2.3)	10.7 (1.7)	12.7 (2.4)
Unit cell edges, Å	a = 98.45	a = 98.29	a = 98.19	a = 98.21
($P2_12_12_1$)	b = 106.46	b = 106.45	b = 106.43	b = 106.57
	c = 535.72	c = 535.25	c = 536.10	c = 535.83
Highest resolution shell, Å	3.53–3.45	3.89–3.80	3.99–3.90	4.20–4.10
R_{work}, %	31.5			36.9
R_{free}, %	35.0			36.6

Multiwavelength anomalous dispersion analysis of ATPγS and ADP crystals. The values in parentheses are for the highest resolution shell. $R_{sym} = \Sigma_{hkl}\Sigma_i |I_i(hkl) - \langle I(hkl)\rangle|/\Sigma_{hkl}\Sigma_i I_i(hkl)$, where $I(hkl)$ is the intensity measurement and $\langle I(hkl)\rangle$ is the mean intensity for multiply recorded reflections. R_{work} and $R_{free} = \Sigma||F_o| - |F_c||/|F_o|$ for the reflections in the working and test sets, respectively. The R_{free} value was calculated by using a randomly selected 10% of the reflections that were omitted during refinement.

Riverside, CA) at 20°C. Crystals were harvested after 24 h, after which time degradation in crystal quality was observed. Optimal cryoprotectant conditions were achieved by soaking the crystals at 4°C in the crystallization medium with increasing amounts of glycerol (5% increments) for 10- to 15-min periods until frozen at 25% glycerol. All cryoprotection buffers included 5 mM ATPγS. The selenomethionine crystals seemed more stable and were harvested after 48 h. The initial ADP-bound crystals were grown by using ATPγS-bound seeds. Additional rounds of ADP-bound crystallization used ADP-bound seeds. Diffraction data were collected at the Advanced Light Source (Berkeley, CA) on beamline 8.2.2.

The crystallographic data are described in Table 1. The crystal structure of the ATPγS-bound clamp-loader complex was solved by multiwavelength anomalous dispersion phasing using standard methods and refined by using data to 3.5 Å (19–25). Crystals grown in the presence of ADP diffracted X-rays to 4.1 Å, and the structure was solved by molecular replacement. Difference Fourier maps clearly show the bound nucleotides (Fig. 2*B*), phosphate groups, and zinc atoms, which were not included in the model until the end of the refinement. Refinement of the ATPγS complex involved positional and temperature-factor optimization at 3.5 Å. The refinement target combined experimental structure factors and phases by using the MLHL option in the program CNS (23). For the ADP complex, only rigid-body optimization at the level of individual domains was performed, along with the optimization of group temperature factors for the backbone and side-chain atoms. Attempts at improving the electron density by using B-factor sharpening were unsuccessful. The coordinates and structure factors for the ATPγS- and ADP-bound structures have been deposited in the Protein Data Bank (PDB ID codes 1XXH and 1XXI, respectively).

ITC. ITC experiments used a MicroCal VP isothermal titration calorimeter (Microcal, Northampton, MA) as described (26). After degassing each sample under vacuum, nucleotide solution containing ATP, ATPγS, ADP, or adenosine 5′-[β,γ-imido]triphosphate (50–150 μM) was titrated into protein solution (2.5–6.1 μM) in 10-μl injections 300 s apart. Raw data for 29 injections at 25°C were obtained by using the Microcal VP-VIEWER software. Control titrations of nucleotide into ITC buffer demonstrated that there was no significant heat of dilution or injection for any of the tested nucleotides (data not shown). Data were analyzed as described (26).

MD Simulations. MD trajectories were generated by using AMBER 6.0 (27) with the PARM98 force field (28). Coordinates for the nonhydrogen atoms of the nucleotide-free clamp-loader complex (6) were used to build hydrogen atoms, adding 23 Na^+ ions to neutralize the total charge. The protonation state of side chains corresponded to that expected for isolated residues at pH 7.0 (except for cysteine residues in the zinc-binding modules, see below). The system was solvated by using a box of transferable intermolecular potential three-point water molecules (29) such that the waters extended out to 9 Å from the protein molecule. Some waters were substituted with Na^+ and Cl^- ions to reflect an ionic strength corresponding to 0.15 M NaCl. The resulting system included four zinc atoms, 23 unpaired Na^+ ions, 137 Na^+/Cl^- pairs, 49,545 water molecules, and 27,885 protein atoms in a box with dimensions 112 × 131 × 144 $Å^3$.

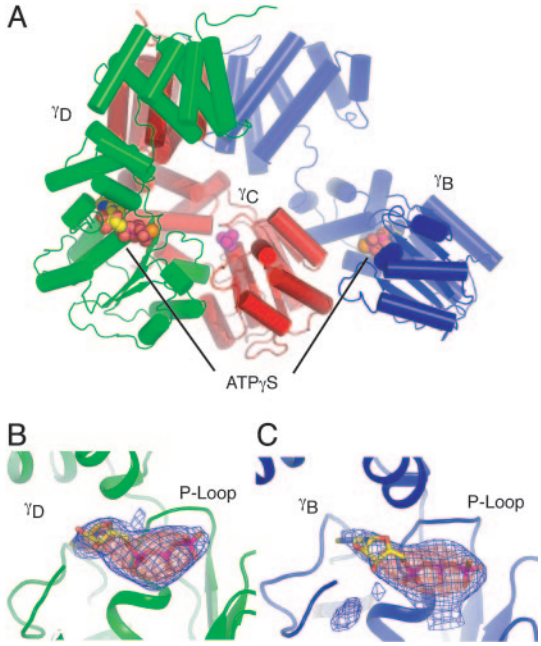

Fig. 2. Ribbon representation of the nucleotide-binding sites in the three γ-subunits. (*A*) Structure of the three γ-subunits. ATPγS is indicated in γ_B and γ_D, and a phosphate ion is bound to γ_C. (*B*) Electron density in a map calculated with amplitudes ($|F_O| - |F_C|$) and phases from a model in which nucleotide is omitted, for the ATPγS complex, site γ_D (blue mesh, 3σ; red mesh, 5σ). (*C*) Electron density in γ_B.

Energy calculations used periodic boundary conditions and the calculation of electrostatic energy using particle-mesh Ewald summations (30). After initial energy minimization, the system was heated to 298 K over a period of 15 ps. Harmonic positional restraints were placed on the protein atoms and reduced gradually over the initial 55 ps of the simulation. The remainder of the MD simulation was carried out in the absence of positional restraints, under constant temperature and pressure conditions. A 2-fs time step was used, with the SHAKE algorithm (31) applied to maintain rigid bond lengths for covalent bonds that include hydrogens. The simulations were generated by using 16–32 processors on an IBM SP2 computer at the National Energy Research Scientific Computing Center (Lawrence Berkeley National Laboratory, Berkeley, CA).

The three γ-subunits and the δ'-subunit (but not δ) each contain a small zinc-binding loop of unknown function that is unique to bacterial clamp loaders (32). In the simulation, the zinc atoms were restrained by covalent bonds to the sulfur atoms, as done in previous simulations of other zinc-containing proteins (33). The charge of the zinc atom was zero, as was the total charge of the cysteine residues. The simulation was extended for a total of 2.0 ns. Typically, 1 ns of simulation took ≈15 days to generate at the National Energy Research Scientific Computing Center.

Results and Discussion

Overall Structure and Crystal Packing. The ATPγS and ADP complexes were obtained in the same crystal form ($P2_12_12_1$; $a \approx 98.4$ Å, $b \approx 106.5$ Å, $c \approx 535.7$ Å), which is distinct from the crystal form of the nucleotide-free structure ($P2_12_12_1$; $a = 95.7$ Å, $b = 95.9$ Å, $c = 285.4$ Å). These crystals contain two clamp-loader complexes in the asymmetric unit, and both are in similar conformations, with two nucleotides bound to each. We previously suggested that the nucleotide-free clamp-loader complex was "held open" by crystal-packing forces and that a stable state for the complex might be a more symmetrical conformation in which δ_A closes over δ'_E. Crystal-packing interactions are substantially different in crystals of the nucleotide-bound and nucleotide-free forms (Fig. 5, which is published as supporting information on the PNAS web site).

The overall conformation of the ATPγS- and ADP-bound clamp-loader complexes, determined by multiwavelength anomalous dispersion phasing and molecular replacement, respectively, are essentially the same as that seen previously for the nucleotide-free state (Fig. 1) (6). For example, in the ATPγS complex, the rms deviation in C^α atoms is 2.03 Å over the entire complex when compared to the nucleotide-free structure. For individual subunits, the rms deviation in C^α atoms between the ATPγS and nucleotide-free structures ranges from 0.86 Å (γ_C) to 2.45 Å (δ_A; small rearrangements in the interdomain orientations account for the larger deviations), after superimposing the individual subunits. This similarity is surprising, because the new structures were obtained in the presence of ATPγS, which has clearly not triggered a significant conformational change, at least as seen in the crystal.

Each complex has two molecules of either ATPγS or ADP bound to it, one to the γ_B-subunit and one to γ_D (Fig. 2). The ATP-binding site on γ_C is occupied by a phosphate ion (data not shown), and nucleotide is excluded because of the close packing of the distal surface of γ_D. The binding of ATPγS to γ_D did not disrupt the closed γ_C–γ_D interface (Fig. 6, which is published as supporting information on the PNAS web site).

Although our structures contain nucleotide, there are no nucleotide-mediated interfacial interactions that stabilize this conformation. A characteristic feature of oligomeric AAA^+ ATPases is the interfacial coordination of ATP by one or more arginine or lysine residues that are presented on the distal surface of the nucleotide-binding domain of the adjacent subunit (9, 10). Clamp-loader subunits contain a conserved arginine located within a Ser-Arg-Cys motif (34), and comparison with the structures of hexameric AAA^+ ATPases and the structure of the RFC:proliferating cell nuclear antigen complex suggest that this arginine could bridge the interface and interact with the third phosphate of ATP (9, 10, 17). This does not happen in our structures, in which the Ser-Arg-Cys motif is in essentially the same position as observed earlier in the nucleotide-free clamp-loader complex (6). The closest interatomic distance between the arginine side chain and the γ phosphate of ATPγS is ≈13 Å. Therefore, we conclude that the asymmetric conformation of the clamp loader, seen previously and observed again in our structures, is a stable state of the clamp loader.

Comparing the clamp-loader complex with the type II, *N*-ethylmaleimide-sensitive factor class of AAA^+ ATPases, p97, it is surprising that conformational changes were not seen, because large conformational changes were observed in p97 in different nucleotide-bound states (35–38). It is interesting that in the nucleotide-bound D2 domain of p97 the arginine finger is also far away from the AlF_3 that mimics the terminal phosphate (36). It may be that the position of the conserved arginine finger determines whether the particular AAA domain is active, or possibly the arginine finger is locked in place until some other cofactor or binding event releases it.

Nucleotide Binding Monitored by ITC. Analysis of the ITC data (Fig. 3) with an independent-site (noncooperative) model yields dissociation constants (K_d) that are similar for ATP and ADP (3.7 and 3.0 μM, respectively), with a stoichiometry of 2 for both nucleotides. These values for K_d are comparable to those obtained for the binding of ATP and ADP to the isolated γ-subunit (26) and suggest that ATP binding to the clamp-loader complex does not convert the complex to a different state, perhaps because of the absence of the clamp and DNA. Although it is possible that the apparent similarity in the binding energy of ATP and ADP reflects the conversion of part of the binding energy of ATP into a conformational change in the clamp loader, the crystal structure of the ATPγS complex suggests instead that the interfacial interactions that recognize ATP may not occur after nucleotide addition in the absence of the clamp. In separate experiments using fluorescence energy transfer measurements we have shown that the clamp-loader complex used here is competent to bind to the clamp in an ATP-dependent manner and that ADP fails to trigger the interaction (16). Unfortunately, the results of ITC experiments in which the β clamp is included are uninterpretable because of nonspecific interactions between ATP and the β clamp in the absence of the clamp loader, leading to nonsaturable isotherms (E. Goedken and J.K., unpublished data). The inner surface of the ring-shaped β clamp is positively charged, and this feature might be responsible for these nonspecific interactions.

The binding of the ATP analogs adenosine 5′-[β,γ-imido]-triphosphate and ATPγS were also monitored by ITC. Adenosine 5′-[β,γ-imido]triphosphate did not bind to the clamp loader, in agreement with previous results (15, 26). ATPγS was found to behave similarly to ATP and binds with a stoichiometry of 2 and K_d of 0.78 μM.

The ITC results are consistent with recent time-resolved measurements of interactions between the *E. coli* clamp loader, clamp, and ATP, which can be interpreted in terms of the binding of two molecules of ATP to the clamp loader in the absence of clamp, with the stoichiometry of ATP binding increasing to 3 in the presence of the clamp (39). Analysis of an archaeal clamp-loader complex with four potential ATP-binding sites suggests that only two ATP molecules are bound in the absence of the clamp, although four are bound in the presence of clamp and DNA (40). Our interpretation of these results is that a cooperative interaction between clamp loader and clamp is required for complete loading of ATP. On the other hand, a Scatchard analysis of [^{32}P]ATP binding to the *E. coli* clamp-loader complex using gel filtration yielded a stoichiometry of 3 in the absence of clamp (34), and the issue of whether the third ATP-binding site in the clamp loader can open in the absence of clamp requires additional study.

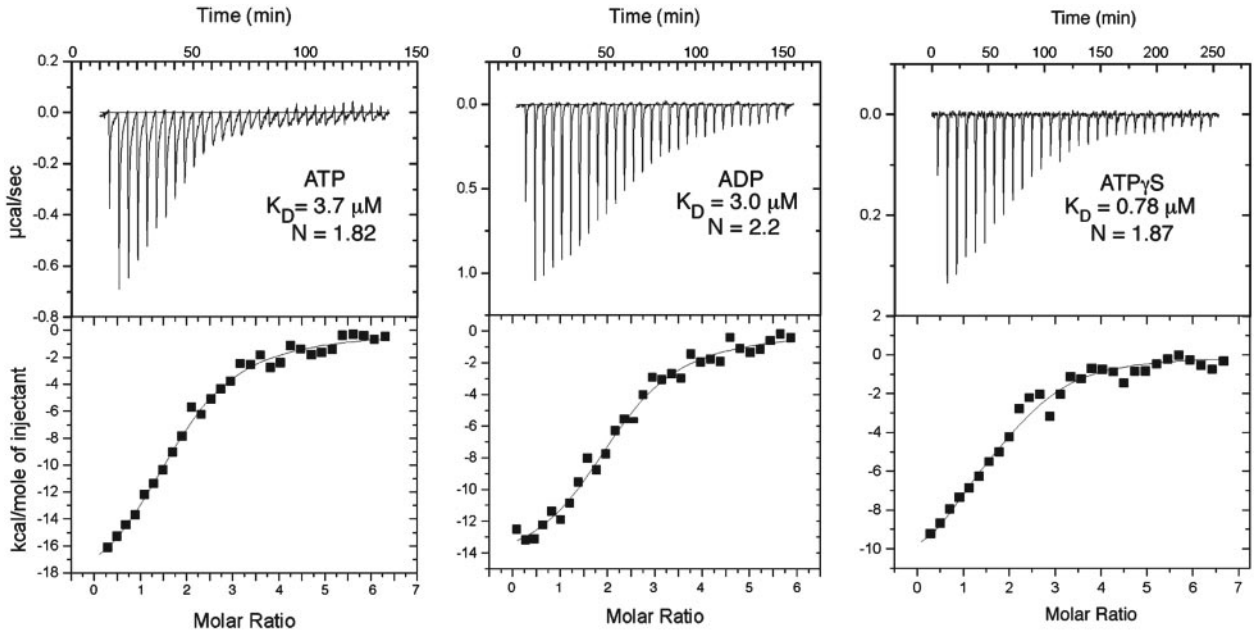

Fig. 3. ITC binding curves for the clamp-loader complex in combination with various nucleotides.

MD Simulations Suggest That the Open Conformation of the Clamp Loader Is Stable in the Absence of ATP. A critical assumption of the earlier analysis of the *E. coli* clamp-loader complex was that the conformation seen in the crystal would relax into a more closed conformation when the constraints of the crystal lattice are released. Although limited to nanosecond time scales, MD simulations can provide insight into the stability of the conformations of protein assemblies [see, for example, studies on the β clamp (14) and the subunits of F_1ATPase (41)]. Therefore, we generated a 2.0-ns MD simulation at 298 K for a fully solvated nucleotide-free clamp-loader complex.

We first analyzed the structural stability of each of the 15 individual domains (three per subunit) in the complex. After allowing 1 ns for equilibration, coordinates were sampled with a time interval of $\Delta t = 0.5$ ps from 1 to 2 ns. For each instantaneous structure, individual domains were superimposed onto the corresponding domain in the crystal structure, thereby generating a time series for structural distortions internal to each domain (Fig. 7, which is published as supporting information on the PNAS web site). The rms deviation in C^{α} positions for domain I of the γ-subunits [excluding the zinc-binding loop (residues 64–79) and an N-terminal region (residues 3–20) that is structurally a part of domain II] is $\approx$1.5 Å at 2.0 ns, and the deviation in the corresponding segments of δ_A and δ'_E is similar (Fig. 7). Similar deviations are seen for domains II and III of all subunits, with no evidence for larger drift in the structures of these domains. These data indicate that the internal structures of the individual domains of the complex are stable during the simulation. The general organizational structure of the clamp-loader complex is also stable during the simulation (data not shown).

Because we had speculated earlier that the clamp-loader complex may be held open by crystal contacts, we examined the simulation for evidence of a collapse of the distance between the δ_A- and δ'_E-subunits. The distance between the centers of mass of domain I of δ_A and δ'_E is $\approx$60 Å in the initial structure, and this distance is never reduced significantly during the simulation. Instead, we find that this distance expands during the simulation to 64.6 Å (1–2 ns) with transient maximum values of >67 Å. This opening of the clamp loader can be traced to segmental motions of domains I and II of δ_A, which are correlated with smaller motions in the corresponding domains of γ_B as well as movements of δ'_E away from δ_A.

An interesting result is obtained if structures from the MD trajectory (which was calculated without the clamp or ATP) are used to model the interaction between the clamp loader and the clamp, based on the known structure of the isolated δ-subunit bound to the β clamp (14). Initially, docking of the clamp-loader complex onto the β clamp results in $\approx$2,500 atomic overlaps (defined as pairs of atoms closer than 2.5 Å) because of collisions between the clamp and subunits C–E of the clamp loader. The outward movement of the δ-subunit during the simulation results in a decrease in the number of atomic overlaps to an average of 2,046 in the 1.0- to 2.0-ns interval (Fig. 4). At 1.1 ns, the number of overlaps reaches a minimum of 1,500, and the distance between the centroids of the domains of δ_A and δ'_E increases to >67 Å. These movements of δ_A and δ'_E bring the δ_A-subunit closer to a confor-

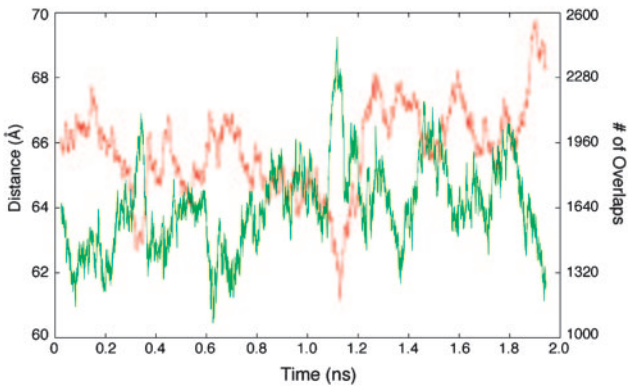

Fig. 4. Results of the MD simulation. The number of atomic overlaps (defined as the number of interatomic contacts with distances <2.5 Å) between the β clamp and clamp loader are displayed for the conformations of clamp loader adopted during the MD simulation (red). Instantaneous structures of the clamp loader from the trajectory were docked individually onto the clamp such that domain I of δ_A matched δ in the crystal structure of the δ:β complex (14). Also shown is the distance (green) between the centers of mass of domain I of δ_A and δ'_E.

mation that can bind to the β clamp without hindrance and suggest that only a gentle "push" may be needed to enable an initial docking of the clamp loader onto the clamp. This picture contrasts with the larger expenditure of energy that might be required to convert the previously postulated closed state, with several sealed intersubunit interfaces, to an open form.

In the original crystal structure of the nucleotide-free clamp loader, it was noted that a tight interface existed between the first two domains of γ_C and γ_D and that this interface would block ATP binding to γ_C (6). A crystal structure of a truncated γ-subunit with ATPγS bound suggested that conformational changes in γ_D after ATP binding would break this tight interface and allow a third ATP to bind to γ_C (26). It is apparent from the crystal structure and ITC data presented here that a conformational change originating solely from ATP binding is not enough to break open this interface or convert the clamp loader to an active conformation. To examine the stability of this interface, the hydrogen-bonding pattern between the subunits was monitored during the MD simulation (there is no significant hydrophobic packing at the interface). Over the last nanosecond of the simulation, persistent hydrogen bonds were observed in two major regions of the γ_C–γ_D interface. The first of these areas involved a patch of residues in domain II of γ_C (residues Asp-216, Ser-219, Gln-223, Ala-226, and Ser-227) with residues in domain I of γ_D (residues Gln-172, His-174, Asn-30, and His-23). A second set of hydrogen bonds involves domain I of γ_C (residues Arg-8, Arg-11, Glu-102, Glu-83, and Arg-86) and γ_D (residues Glu-144, Arg-133, Arg-169, and Asn-137). These interactions seem to define one of the intersubunit latches that hold the inactive structure in a stable form.

Concluding Remarks

Our original analysis of the first clamp-loader structure led to a simple model in which ATP binding and hydrolysis were coupled to the release and subsequent sequestration of a single clamp-opening subunit δ_A (6, 12, 15). The structure showed that the ATPase domains of the clamp loader were arranged in an asymmetric and splayed-out arrangement, with the δ_A-subunit in an exposed orientation. Only minimal adjustments in the orientation of the δ_A-subunit would be required to allow it to have unimpeded access to the surface of the β clamp. Because the δ-subunit can open the clamp on its own, it was proposed that ATP binding would be required to drive the clamp loader from a more closed conformation to an open form resembling the crystal structure, in which the δ_A-subunit would be fully released to interact with the clamp.

The results presented here suggest that the clamp-loading cycle is likely to be more complex. The conformation of the clamp loader seen originally in the crystals of the nucleotide-free form is likely to be a stable state. Comparison with the structure of the RFC complex bound to proliferating cell nuclear antigen suggests that the aspect of the conformation of the clamp loader that is incompatible with docking onto the clamp has most likely to do with the γ-subunits, which are not positioned appropriately in the structure, rather than just the δ_A subunit orientation. The third ATP-binding site at γ_C in the bacterial clamp loader is blocked by the extensive interface between γ_C and γ_D. It might be that only two ATP molecules are readily bound by the clamp loader in the absence of clamp and that the γ_C–γ_D interface acts as an autoinhibitory mechanism that minimizes the futile hydrolysis of ATP. ATP binding might drive a cooperative structural transition that results in an extensive interaction between several subunits of the clamp loader and the clamp, as suggested by recent biochemical data (42).

The available crystal structures provide snapshots of an inactive state of the bacterial clamp loader, described here and in our earlier article (6), and a state of the eukaryotic clamp loader that is likely to resemble the situation just before hydrolyzing ATP and releasing the closed clamp on DNA (17). What is missing is a direct view of the ATP-bound form of the clamp loader interacting with an open clamp. Such a view would provide an important linkage between two terminal states of the ATP-dependent process that are now reasonably well understood.

We thank the staff of the Advanced Light Source (Department of Energy, Lawrence Berkeley National Laboratory), particularly Corie Ralston and Thomas Earnest, for help with the crystallography. Mass spectrometry was performed by David King. We thank David Jeruzalmi, Bhushan Nagar, Gregory Bowman, Eric Goedken, Holger Sondermann, Matthew Young, Aaron Johnson, Byron DeLaBarre, and Axel Brünger for helpful conversations and advice and Lore Leighton for the schematic diagram. This work was supported in part by National Institutes of Health Grants GM45547 (to J.K.) and GM38839 (to M.O.D.). This work was also supported by Department of Energy Grant DOEDEAC03-7600098 (to the Advanced Light Source and the National Energy Research Scientific Computing center at Lawrence Berkeley National Laboratory for supercomputer work).

1. Stukenberg, P. T., Studwell-Vaughan, P. S. & O'Donnell, M. (1991) *J. Biol. Chem.* **266,** 11328–11334.
2. Stillman, B. (1994) *Cell* **78,** 725–728.
3. Kelman, Z. & O'Donnell, M. (1995) *Annu. Rev. Biochem.* **64,** 171–200.
4. Jeruzalmi, D., O'Donnell, M. & Kuriyan, J. (2002) *Curr. Opin. Struct. Biol.* **12,** 217–224.
5. Millar, D., Trakselis, M. A. & Benkovic, S. J. (2004) *Biochemistry* **43,** 12723–12727.
6. Jeruzalmi, D., O'Donnell, M. & Kuriyan, J. (2001) *Cell* **106,** 429–441.
7. Oyama, T., Ishino, Y., Cann, I. K., Ishino, S. & Morikawa, K. (2001) *Mol. Cell* **8,** 455–463.
8. Neuwald, A. F., Aravind, L., Spouge, J. L. & Koonin, E. V. (1999) *Genome. Res.* **9,** 27–43.
9. Yu, R. C., Hanson, P. I., Jahn, R. & Brunger, A. T. (1998) *Nat. Struct. Biol.* **5,** 803–811.
10. Lenzen, C. U., Steinmann, D., Whiteheart, S. W. & Weis, W. I. (1998) *Cell* **94,** 525–536.
11. Hingorani, M. M. & O'Donnell, M. (1998) *J. Biol. Chem.* **273,** 24550–24563.
12. Naktinis, V., Onrust, R., Fang, L. & O'Donnell, M. (1995) *J. Biol. Chem.* **270,** 13358–13365.
13. Onrust, R., Stukenberg, P. T. & O'Donnell, M. (1991) *J. Biol. Chem.* **266,** 21681–21686.
14. Jeruzalmi, D., Yurieva, O., Zhao, Y., Young, M., Stewart, J., Hingorani, M., O'Donnell, M. & Kuriyan, J. (2001) *Cell* **106,** 417–428.
15. Turner, J., Hingorani, M. M., Kelman, Z. & O'Donnell, M. (1999) *EMBO J.* **18,** 771–783.
16. Goedken, E. R., Levitus, M., Johnson, A., Bustamante, C., O'Donnell, M. & Kuriyan, J. (2004) *J. Mol. Biol.* **336,** 1047–1059.
17. Bowman, G. D., O'Donnell, M. & Kuriyan, J. (2004) *Nature* **429,** 724–730.
18. Miyata, T., Oyama, T., Mayanagi, K., Ishino, S., Ishino, Y. & Morikawa, K. (2004) *Nat. Struct. Mol. Biol.* **11,** 632–636.
19. Otwinowski, Z. & Minor, W. (1997) DENZO (Univ. of Texas, Southwestern Medical Center, Dallas).
20. Collaborative Computational Project Number (1994) *Acta Crystallogr. D* **50,** 760–763.
21. Terwilliger, T. C. & Berendzen, J. (1999) *Acta Crystallogr. D* **55,** 849–861.
22. de La Fortelle, E. & Bricogne, G. (1996) in *Methods in Enzymology*, eds. Carter, C. W. & Sweet, R. M. (Academic, New York), Vol. 276, pp. 472–494.
23. Brünger, A. T., Adams, P. D., Clore, G. M., DeLano, W. L., Gros, P., Grosse-Kunstleve, R. W., Jiang, J. S., Kuszewski, J., Nilges, M., Pannu, N. S., *et al.* (1998) *Acta Crystallogr. D* **54,** 905–921.
24. Navaza, J. (1994) *Acta Crystallogr. A* **50,** 157–163.
25. Jones, T. A., Zou, J.-Y., Cowan, S. W. & Kjeldgaard, M. (1991) *Acta Crystallogr. A* **47,** 110–119.
26. Podobnik, M., Weitze, T. F., O'Donnell, M. & Kuriyan, J. (2003) *Structure (London)* **11,** 253–263.
27. Case, D. A., Pearlman, D. A., Caldwell, J. W., Cheatham, T. E. I., Ross, W. S., Simmerling, C., Darden, T., Merz, K. M., Stanton, R. V., Cheng, A., *et al.* (1999) AMBER (Univ. of California, San Francisco), Version 6.0.
28. Cheatham, T. E. I., Cielplak, P. & Kollman, P. A. (1999) *J. Biomol. Struct. Dyn.* **16,** 845–862.
29. Jorgensen, W. L. (1981) *J. Am. Chem. Soc.* **103,** 335–340.
30. Darden, T., York, D. & Pedersen, L. (1995) *J. Chem. Phys.* **98,** 10089–10092.
31. Ryckaert, J. P., Ciccotti, G. & Berendsen, H. J. C. (1977) *J. Comput. Phys.* **23,** 327–336.
32. Guenther, B., Onrust, R., Sali, A., O'Donnell, M. & Kuriyan, J. (1997) *Cell* **91,** 335–345.
33. Lee, M. S., Gippert, G. P., Soman, K. V., Case, D. A. & Wright, P. E. (1989) *Science* **245,** 635–637.
34. Johnson, A. & O'Donnell, M. (2003) *J. Biol. Chem.* **278,** 14406–14413.
35. Rouiller, I., DeLaBarre, B., May, A. P., Weis, W. I., Brünger, A. T., Milligan, R. A. & Wilson-Kubalek, E. M. (2002) *Nat. Struct. Biol.* **9,** 950–957.
36. DeLaBarre, B. & Brünger, A. T. (2003) *Nat. Struct. Biol.* **10,** 856–863.
37. Huyton, T., Pye, V. E., Briggs, L. C., Flynn, T. C., Beuron, F., Kondo, H., Ma, J., Zhang, X. & Freemont, P. S. (2003) *J. Struct. Biol.* **144,** 337–348.
38. Zhang, X., Shaw, A., Bates, P. A., Newman, R. H., Gowen, B., Orlova, E., Gorman, M. A., Kondo, H., Dokurno, P., Lally, J., *et al.* (2000) *Mol. Cell* **6,** 1473–1484.
39. Williams, C. R., Snyder, A. K., Kuzmic, P., O'Donnell, M. & Bloom, L. B. (2004) *J. Biol. Chem.* **279,** 4376–4385.
40. Seybert, A. & Wigley, D. B. (2004) *EMBO J.* **23,** 1360–1371.
41. Böckmann, R. A. & Grubmüller, H. (2003) *Biophys. J.* **85,** 1482–1491.
42. Leu, F. P. & O'Donnell, M. (2001) *J. Biol. Chem.* **276,** 47185–47194.
43. DeLano, W. L. (1998) The PYMOL Molecular Graphics System (DeLano Scientific, San Carlos, CA).